



HAL
open science

The prompt-early afterglow connection in gamma-ray bursts: implications for the early afterglow physics

R. Hascoët, F. Daigne, R. Mochkovitch

► **To cite this version:**

R. Hascoët, F. Daigne, R. Mochkovitch. The prompt-early afterglow connection in gamma-ray bursts: implications for the early afterglow physics. *Monthly Notices of the Royal Astronomical Society*, 2014, 442, pp.20-27. 10.1093/mnras/stu750 . insu-03645361

HAL Id: insu-03645361

<https://insu.hal.science/insu-03645361>

Submitted on 25 Apr 2022

HAL is a multi-disciplinary open access archive for the deposit and dissemination of scientific research documents, whether they are published or not. The documents may come from teaching and research institutions in France or abroad, or from public or private research centers.

L'archive ouverte pluridisciplinaire **HAL**, est destinée au dépôt et à la diffusion de documents scientifiques de niveau recherche, publiés ou non, émanant des établissements d'enseignement et de recherche français ou étrangers, des laboratoires publics ou privés.

The prompt–early afterglow connection in gamma-ray bursts: implications for the early afterglow physics

R. Hascoët,¹★ F. Daigne² and R. Mochkovitch²

¹Physics Department and Columbia Astrophysics Laboratory, Columbia University, 538 West 120th Street, New York, NY 10027, USA

²UPMC-CNRS, UMR7095, Institut d’Astrophysique de Paris, F-75014 Paris, France

Accepted 2014 April 13. Received 2014 April 4; in original form 2014 January 3

ABSTRACT

The early X-ray afterglow of gamma-ray bursts revealed by *Swift* carried many surprises. Following an initial steep decay the light curve often exhibits a plateau phase that can last up to several 10^4 s, with in addition the presence of flares in 50 per cent of the cases. We focus in this paper on the plateau phase whose origin remains highly debated. We confront several newly discovered correlations between prompt and afterglow quantities (isotropic emitted energy in gamma-rays, luminosity and duration of the plateau) to several models proposed for the origin of plateaus in order to check if they can account for these observed correlations. We first show that the scenario of plateau formation by energy injection into the forward shock leads to an efficiency crisis for the prompt phase and therefore study two possible alternatives: the first one still takes place within the framework of the standard forward shock model but allows for a variation of the microphysics parameters to reduce the radiative efficiency at early times; in the second scenario the early afterglow results from a long-lived reverse shock. Its shape then depends on the distribution of energy as a function of Lorentz factor in the ejecta. In both cases, we first present simple analytical estimates of the plateau luminosity and duration and then compute detailed light curves. In the two considered scenarios we find that plateaus following the observed correlations can be obtained under the condition that specific additional ingredients are included. In the forward shock scenario, the preferred model supposes a wind external medium and a microphysics parameter ϵ_e that first varies as $n^{-\xi}$ (n being the external density), with $\xi \sim 1$ to get a flat plateau, before staying constant below a critical density n_0 . To produce a plateau in the reverse shock scenario the ejecta must contain a tail of low Lorentz factor with a peak of energy deposition at $\Gamma \gtrsim 10$.

Key words: radiation mechanisms: non-thermal – shock waves – gamma-ray burst: general.

1 INTRODUCTION

Before the launch of the *Swift* satellite (Gehrels et al. 2004) the afterglow was believed to be the best understood part of gamma-ray burst (GRB) physics, being explained by the energy dissipated in the forward shock formed by the jet impacting the burst environment (Meszaros & Rees 1997; Sari, Piran & Narayan 1998). However, the many surprises of the early X-ray afterglow revealed by *Swift* – initial steep decay, plateau phase, flares – have considerably complicated the picture (Nousek et al. 2006; O’Brien et al. 2006).

Several mechanisms have been proposed to explain the plateau, the most popular being energy injection into the forward shock (Rees & Meszaros 1998; Sari & Mészáros 2000; Nousek et al.

2006) resulting from a long-lasting activity of the central engine (which could be also responsible for the flares; Zhang et al. 2006) or from a wide distribution of Lorentz factors in the ejecta. Other possibilities include (i) direct emission from a magnetar (e.g. Rowlinson et al. 2013), (ii) coasting of the external blast wave in a wind medium (e.g. Shen & Matzner 2012), (iii) varying microphysics parameters (Granot, Königl & Piran 2006; Ioka et al. 2006), (iv) reverse shock contribution (Genet, Daigne & Mochkovitch 2007; Uhm & Beloborodov 2007). In (i) the end of the plateau corresponds to the spin-down time of the protomagnetar or its collapse to a black hole. Therefore this scenario is mostly promising to explain peculiar plateaus that are followed by a steep decay (temporal index ~ -2 or steeper), while ‘standard’ plateaus (followed by a temporal decay index ~ -1.5) are most likely of afterglow origin; (ii) requires the Lorentz factor of the ejecta to be at most a few tens (so that the coasting phase lasts long enough), which is in severe tension with the minimum Lorentz factor of the ejecta derived from the

★ E-mail: hascoet@astro.columbia.edu

compactness constraint (e.g. Lithwick & Sari 2001; Hascoët et al. 2012). In this work we focus on cases (iii) and (iv) in connection with the recent discovery of correlations between prompt and afterglow quantities (Dainotti, Ostrowski & Willingale 2011; Dainotti et al. 2013; Grupe et al. 2013; Margutti et al. 2013). We especially want to explore if these correlations can be satisfied by the models and which kind of constraints do they impose.

We first summarize in Section 2 the observational results on the prompt–afterglow correlations and in Section 3 we show that explaining the plateau by late energy injection into the forward shock leads to an ‘efficiency crisis’ for the prompt phase. We then consider in Section 4 the possibility that the microphysics parameters in the forward shock vary during the early afterglow and in Section 5 we explore the alternative model where the afterglow is made by the reverse shock. Our results are discussed in Section 6, which is also the conclusion.

2 THE PROMPT–AFTERGLOW CONNECTION

For events with a measured redshift and a well-defined plateau phase, quantities such as t_p – duration of the plateau in the burst rest frame, L_p – luminosity at the end of the plateau or E_X – energy released in X-rays during the plateau, can be measured together with the isotropic energy in gamma-rays of the prompt phase $E_{\gamma,\text{iso}}$. From the samples recently analysed by Dainotti et al. (2011, 2013) and Margutti et al. (2013) some clear correlations appear between prompt and afterglow quantities.¹ The plateau luminosity L_p and energy E_X increase with $E_{\gamma,\text{iso}}$ and decrease for larger t_p . Since an increase of L_p and E_X with $E_{\gamma,\text{iso}}$ could be expected, we also consider below the ratios $L_p/E_{\gamma,\text{iso}}$ and $E_X/E_{\gamma,\text{iso}}$, which, respectively, decrease and barely evolve with increasing t_p .

These prompt–afterglow correlations represent potentially important clues to understand the many surprises of the early afterglow. In the standard forward shock scenario (for a wide range of parameters) the X-ray flux depends on the energy injected into the shock and the microphysics, but not on the density of external medium. In the reverse shock scenario the shape of the early afterglow depends both on the density of the burst environment and on the distribution of energy in the ejecta that is crossed by the reverse shock. Below, we investigate under which conditions the observed correlations can be reproduced in the framework of these two scenarios.

3 MAKING A PLATEAU WITH LATE ENERGY INJECTION

Continuous energy injection into the forward shock (Rees & Meszaros 1998; Sari & Mészáros 2000; Nousek et al. 2006) is commonly invoked to account for plateau formation. For the most extended plateaus it however imposes to inject up to several hundred times the energy that was initially present to power the prompt phase. This is illustrated in Fig. 1 where we have plotted X-ray light curves all with the same initial injected energy $E_0 = 10^{52}$ erg but where the final energy is 2, 10 or 100 times larger. It is only in this last case that a plateau lasting several hours can be obtained. Energy injection into the forward shock can take place in two ways: either

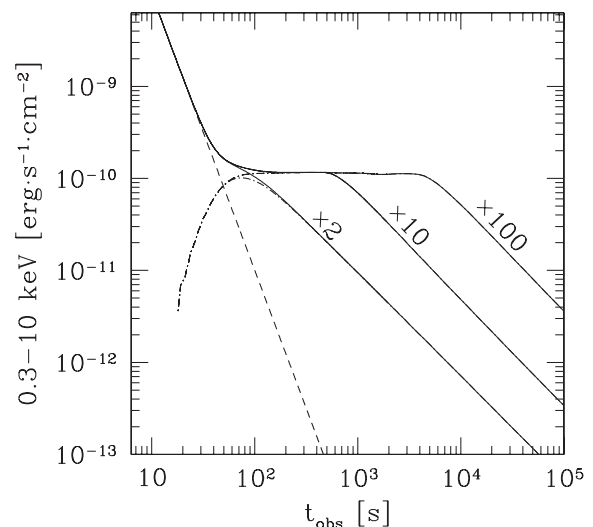


Figure 1. X-ray afterglow light curves from late energy injection into the forward shock. The initial energy in the shock is $E_0 = 10^{52}$ erg and the three light curves correspond (from left to right) to a final energy being, respectively, 2, 10 and 100 times larger. The dashed line represents the continuation of the early steep decay that terminates the prompt emission, while the dash-dotted line shows the forward shock emission only. A redshift $z = 1$, a uniform external medium of density $n = 10 \text{ cm}^{-3}$, and constant microphysics parameters $\epsilon_e = 0.1$ and $\epsilon_B = 0.01$ have been assumed.

the source stays active during the whole duration of the plateau or it is short lived but has produced a tail of low Lorentz factor material that is progressively catching up, adding energy to the shock. We have considered this latter case to obtain Fig. 1 (the source being active for 10 s) but the former one gives similar results.

The huge amount of energy to be injected after the end of the prompt phase leads to an ‘efficiency crisis’ for the prompt mechanism. The measured gamma-ray efficiency is

$$f_{\gamma,\text{mes}} = \frac{E_\gamma}{E_\gamma + E_{\text{fs}}}, \quad (1)$$

where the energy in the forward shock, E_{fs} , is estimated from multi-wavelength fits of the afterglow typically after 1 d (i.e. after energy injection; see e.g. Zhang et al. 2007). However, the true efficiency is

$$f_{\gamma,\text{true}} = \frac{E_\gamma}{E_\gamma + E_{\text{fs},0}} = \frac{1}{1 + \frac{1}{k} \left(\frac{1}{f_{\gamma,\text{mes}}} - 1 \right)}, \quad (2)$$

where $E_{\text{fs},0}$ is the energy initially present (after the prompt phase and before the beginning of energy injection) in the forward shock and $k = E_{\text{fs}}/E_{\text{fs},0} \gg 1$. With for example $f_{\gamma,\text{mes}} = 0.1$, the true efficiency is $f_{\gamma,\text{true}} = 0.53$ for $k = 10$ and 0.92 for $k = 100$. These values of $f_{\gamma,\text{true}}$ seems unreachable for any of the proposed prompt mechanisms: the efficiency of internal shocks can barely reach 10 per cent (e.g. Rees & Meszaros 1994; Kobayashi, Piran & Sari 1997; Daigne & Mochkovitch 1998) while that of Comptonized photosphere (e.g. Rees & Mészáros 2005; Beloborodov 2010) or reconnection (e.g. Spruit, Daigne & Drenkhahn 2001; Drenkhahn & Spruit 2002) models is more uncertain but certainly cannot exceed 50 per cent.

¹ The existence of such correlations was already suggested by the pre-*Swift* study of Boër & Gendre (2000) and by Gendre, Galli & Boër (2008), who discovered a correlation between the brightness of the X-ray afterglow and its decay rate at 0.1–10 d.

4 MAKING A PLATEAU AVOIDING AN ENERGY CRISIS

4.1 Forward shock scenario

The standard forward shock scenario can successfully account for the afterglow evolution after about 1 d but fails to reproduce the plateau phase. A backwards extrapolation of the late afterglow flux lies above the plateau, which might therefore be interpreted as the indication that some normally expected radiation is ‘missing’. This can be the case if the radiative efficiency of the forward shock during the early afterglow is smaller than assumed by the simplest version of the standard model. The most obvious way to reduce the efficiency is to relax the assumption that the microphysics parameters stay constant throughout the whole afterglow evolution (Granot et al. 2006; Ioka et al. 2006).

For both a uniform and a wind external medium the afterglow X-ray flux behaves as (Panaitescu & Kumar 2000)

$$F_X \propto E^{\frac{p+2}{4}} \epsilon_e^{p-1} \epsilon_B^{\frac{p-2}{4}} t^{-\frac{3p-2}{4}}, \quad (3)$$

where E is the burst isotropic energy, ϵ_e and ϵ_B are the microphysics parameters and p is the power-law index of the accelerated electron spectrum. Equation (3) is valid as long as the X-ray frequency is larger than both the injection and cooling frequencies, which is generally the case.

With $2 < p < 3$ the dependence on ϵ_B is weak so that in practice only playing with ϵ_e can really affect the flux evolution. A priori ϵ_e can be a function of the shock Lorentz factor, the density of the external medium (in the case of a stellar wind) or both. The stellar wind case is of special interest if we make the simple assumption that, below a critical density n_0 , ϵ_e is constant while $\epsilon_e \propto n^{-\xi}$ (with $\xi > 0$) for $n > n_0$. Since the density seen by the forward shock is given by

$$n(t) \simeq \frac{4\pi c}{m_p} \frac{A^2}{E t} \simeq 5.6 \cdot 10^2 A_*^2 E_{53}^{-1} t_3^{-1} \text{ cm}^{-3}, \quad (4)$$

where t is the (redshift-corrected) observer time and A_* is the wind density normalization ($\rho(r) = A/R^2$ with $A = 5 \times 10^{11} A_* \text{ g cm}^{-1}$) the transition at n_0 , which marks the end of the plateau, takes place at

$$t_p \approx 5.6 \cdot 10^5 A_*^2 n_0^{-1} f_\gamma E_{\gamma,53}^{-1} \text{ s}, \quad (5)$$

where f_γ is the gamma-ray efficiency of the prompt phase and $E_{\gamma,53}$ is the isotropic gamma-ray energy release. Then, if the product $A_*^2 n_0^{-1} f_\gamma$ typically stays in the range $3 \times 10^{-4} - 3 \times 10^{-2}$ the resulting $[t_p, E_{\gamma,\text{iso}}]$ sequence can accommodate most of the bursts in the Margutti et al. (2013) sample (see Fig. 5).

A flat plateau is expected for

$$\xi = \xi_0 = \frac{3p-2}{4(p-1)} = 1 - \frac{p-2}{4(p-1)} \approx 1 \quad (6)$$

while for $\xi < \xi_0$ (resp. $\xi > \xi_0$) the plateau flux is decreasing (resp. rising) with time.

With $\epsilon_e \propto n^{-1}$ and from equation (3), a flat plateau extending over two decades in time requires an increase of ϵ_e by a factor of about 100 from the beginning to the end of the plateau. It is beyond the scope of this paper to decide if this is indeed possible but it is remarkable that acting on one single parameter can lead to the formation of a plateau that also satisfies the observed prompt-afterglow correlations (see Section 5.1).

The other possibility where ϵ_e depends on the Lorentz factor does not yield satisfactory results. Assuming that the transition from a

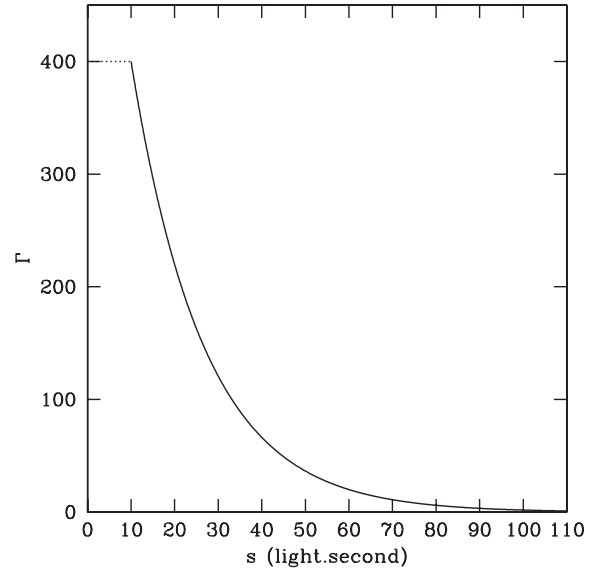


Figure 2. Lorentz factor in the ejecta as a function of the distance from the front (in light.seconds). The ‘head’ (from 0 to 10 light.seconds) is made of material with typical Lorentz factor $\bar{\Gamma} = 400$ while in the tail Γ decreases from 400 to unity following equation (8), so that $\frac{dE}{d\log\Gamma}$ is constant.

varying to a constant ϵ_e takes place at a fixed Γ , the deceleration laws of the blast wave

$$\Gamma \propto \begin{cases} \left(\frac{E}{n}\right)^{1/8} t^{-3/8} & \text{uniform medium} \\ \left(\frac{E}{A}\right)^{1/4} t^{-1/4} & \text{wind} \end{cases} \quad (7)$$

then lead to $t_p \propto E_\gamma^{1/3}$ and $t_p \propto E_\gamma$ in the uniform medium and wind cases, respectively, showing a trend opposite to the observed one.

4.2 Reverse shock scenario

We now suppose that the ejecta emitted by the central engine is made of a ‘head’ with material at high Lorentz factors ($\Gamma \sim 10^2 - 10^3$), followed by a ‘tail’ where the Lorentz factor decreases to much smaller values, possibly close to unity. The head is responsible for the prompt emission while the reverse shock propagating through the tail makes the afterglow.

We adopt for the head a constant energy injection rate \dot{E}_H for a duration of 10 s. We do not specify the distribution of the Lorentz factor and simply consider its average value, supposed to be $\bar{\Gamma} = 400$. The tail that follows lasts for 100 s but this value is not critical as long as it remains sufficiently short not to exceed the duration of the early steep decay phase observed at the beginning of most X-ray light curves. We start with a simple case where the distribution of energy in the tail $\frac{dE}{d\log\Gamma}$ is constant from $\Gamma = 400$ to 1. This can be obtained by adopting a constant energy injection rate \dot{E}_T and a Lorentz factor of the form

$$\Gamma_T(s) = 400^{1.1-s/100\text{s}}, \quad (8)$$

from $s = 10$ to 110 light.seconds, the distance s being counted from the front to the back of the flow (see Fig. 2).

Using the methods described in Genet et al. (2007) we have obtained the power $P_{\text{diss}}(t)$ dissipated by the reverse shock as a function of arrival time to the observer for $E_H = 10\dot{E}_T = 5 \cdot 10^{52} \text{ erg s}^{-1}$ (so that equal amounts of energy are injected in the head and tail) and two possibilities for the burst environment: (i) a uniform medium with $n = 1000 \text{ cm}^{-3}$ (supposed to be representative of a massive star

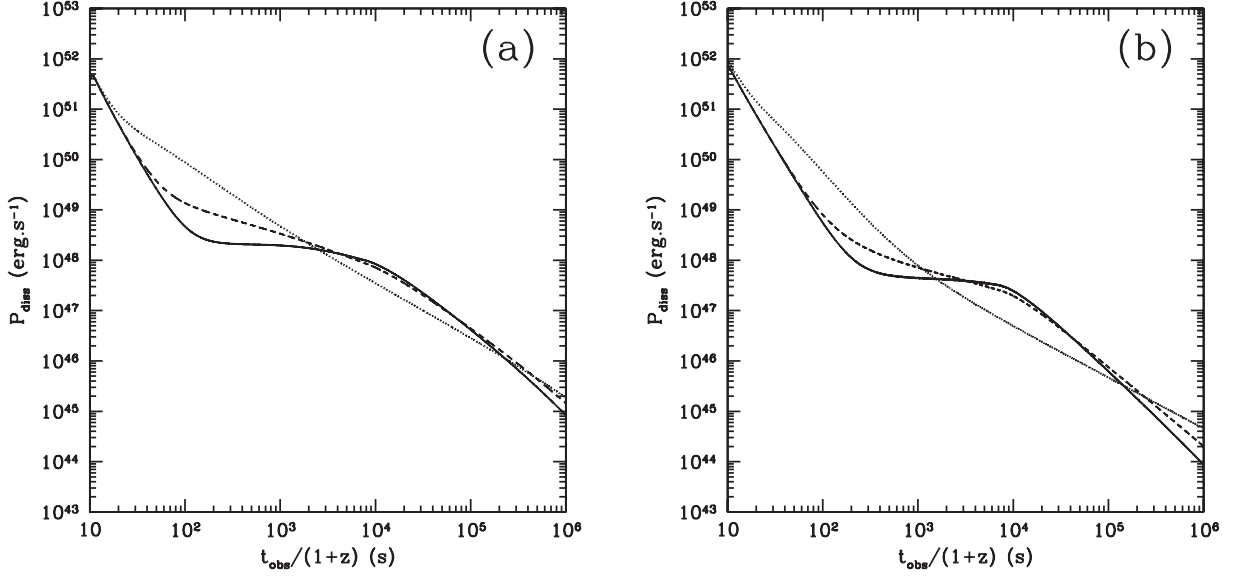


Figure 3. Dissipated power in the reverse shock as a function of observer time for equal amounts of energy $E_H = E_T = 5 \cdot 10^{53}$ erg in the head and tail. The distribution of energy in the tail as a function of Lorentz factor is given by equation (9). (a): uniform external medium of density $n = 1000 \text{ cm}^{-3}$, $\Gamma_* = 12$, $q = q' = 1.5$ (dashed line) and $q = q' = 2.5$ (full line); (b): stellar wind with $A_* = 1$, $E_H = E_T = 5 \cdot 10^{53}$ erg, $\Gamma_* = 20$, $q = q' = 3$ (dashed line) and $q = q' = 4.5$ (full line). In both panels, the dotted lines have $q = q' = 0$ and correspond to a uniform distribution of energy $\frac{dE}{d\text{Log}\Gamma}$ in the tail.

environment) or (ii) a stellar wind with a wind parameter $A_* = 1$. Going from the dissipated power to actual light curves depends on the assumptions that have to be made for the microphysics parameters. The general shape of the early X-ray afterglow light curves however remains globally similar to the evolution of $P_{\text{diss}}(t)$ so that some conclusions can already be reached without having to consider the uncertain post-shock microphysics.

Fig. 3 (dotted curves) shows that if energy is evenly distributed in the tail (constant $\frac{dE}{d\text{Log}\Gamma}$) the dissipated power approximately decays as t^{-1} after about 1000 s, for both a uniform and a wind ambient medium. The contrast $\kappa = \Gamma/\Gamma_{\text{bw}}$, where Γ and Γ_{bw} are, respectively, the Lorentz factors of the unshocked ejecta and the blast wave, is larger for the uniform medium than for the wind case ($\kappa \simeq 2$ and $\sqrt{2}$, respectively; see Genet et al. 2007). As seen in Fig. 3 the dissipated power is therefore larger (by a factor of 3–5) in the uniform medium.

We now vary the energy deposition in the tail, concentrating more power at some value of the Lorentz factor. We have for example considered a simple model where

$$\dot{E}_{\text{T}}(\Gamma) = \begin{cases} \dot{E}_* \left(\frac{\Gamma}{\Gamma_*}\right)^{-q} & \text{for } \Gamma > \Gamma_* \\ \dot{E}_* \left(\frac{\Gamma}{\Gamma_*}\right)^{q'} & \text{for } \Gamma < \Gamma_* \end{cases} \quad (9)$$

the value of \dot{E}_* being fixed by the total energy injected in the tail. Figs 3(a) and (b), respectively, show the dissipated power for $\Gamma_* = 12$, $q = q' = 1.5$ and 2.5 (uniform medium) and $\Gamma_* = 20$, $q = q' = 3$ and 4.5 (stellar wind) with $E_H = E_T$ in both cases. When energy deposition is more concentrated (increasing q and q') a plateau progressively forms and becomes flatter. The value of Γ_* in equation (9) fixes the duration of the plateau as it corresponds to the time when the reverse shock reaches s_* , where $\Gamma_{\text{T}}(s_*) = \Gamma_*$. The q parameter controls the flatness of the plateau while q' controls the decay index after the plateau.

The duration t_p of the plateau is roughly given by

$$t_p \sim \begin{cases} 6 \times 10^5 E_{\text{H},53}^{1/3} n^{-1/3} \Gamma_{*,1}^{-8/3} \text{ s} \\ 10^5 E_{\text{H},53} A_*^{-1} \Gamma_{*,1}^{-4} \text{ s} \end{cases} \quad (10)$$

for a uniform and wind medium, respectively. Equation (10) corresponds to the situation of a decelerating shell that does not receive any supply of energy, contrary to the present case where material from the tail is continuously catching up. It however remains approximately correct as long as E_T does not largely exceed the energy E_H in the head of the ejecta (as it happens in models where the plateau is made by energy injection into the forward shock discussed in Section 3).

An analytical solution corresponding to the results of Fig. 3 can be obtained from the following expression of P_{diss} (Genet et al. 2007)

$$P_{\text{diss}} = \frac{dM}{d\Gamma} \frac{d\Gamma}{dt} \Gamma e c^2, \quad (11)$$

where $M(\Gamma)$ gives the distribution of mass as a function of the Lorentz factor in the tail, $\Gamma(t)$ is the Lorentz factor of the tail material just being shocked at observer time t (without the $(1+z)$ time dilation factor) and e is the fraction of the incoming material kinetic energy dissipated in the reverse shock. From equation (9) we get

$$\frac{dM}{d\Gamma} = \frac{\dot{E}_*}{\Gamma_* c^3} \left(\frac{\Gamma}{\Gamma_*}\right)^{\pm q-1} \frac{ds}{d\Gamma} = \frac{\dot{E}_* \tau}{\Gamma_* c^2} \left(\frac{\Gamma}{\Gamma_*}\right)^{\pm q-1} \times \frac{1}{\Gamma}, \quad (12)$$

with $\tau = 100/\ln 400$ s [we do not distinguish between q and q' in equation (12) to simplify the notation]. The total energy in the tail is given by

$$E_T = \int_{10}^{110} \dot{E}_{\text{T}} dt = \dot{E}_* \tau \times \varphi_{qq'}, \quad (13)$$

with

$$\varphi_{qq'} = \frac{1}{q} + \frac{1}{q'}. \quad (14)$$

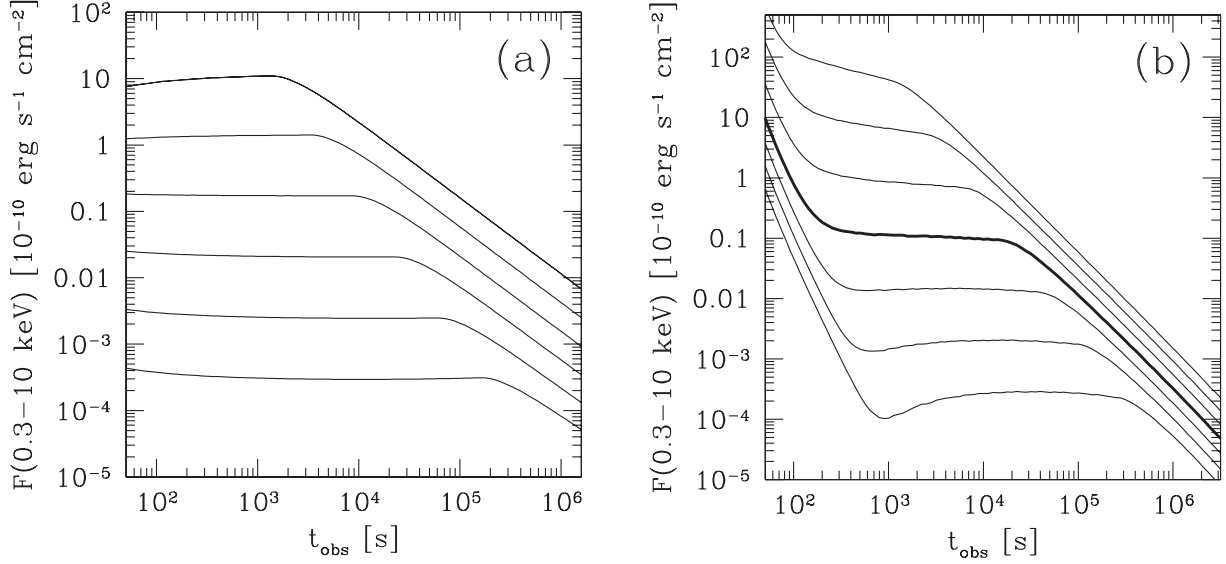


Figure 4. Sequences of X-ray afterglow light curves with plateaus. (a): forward shock scenario with $\epsilon_e \propto n^{-1}$ for $n > n_0 = 15 \text{ cm}^{-3}$, a wind parameter $A_* = 0.5$ and a gamma-ray efficiency $f_\gamma = 0.2$. The bottom curve corresponds to an energy injected into the forward shock of $8.5 \times 10^{51} \text{ erg}$ and the others to successive multiplication of the energy by a factor $F = 2.5$; (b): reverse shock scenario with $\epsilon_e = 0.1$, $\epsilon_B = 0.01$, an external medium of uniform density $n = 1000 \text{ cm}^{-3}$, a distribution of power in the tail given by equation (9) with $q = 8/3$ and $q' = 4/3$. The thick light curve has $E_H = E_T = 2 \times 10^{54} \text{ erg}$ and $\Gamma_* = 16$, while the three others above (resp. below) are obtained by successively multiplying (resp. dividing) the energies by $F = 2.5$ and the Lorentz factors by $F^{1/2}$. In both panels an index $p = 2.2$ for the electron spectrum and a redshift $z = 1$ have been assumed.

We now write $\Gamma(t)$ as

$$\Gamma(t) \simeq \Gamma_* \left(\frac{t}{t_p} \right)^{-\gamma}, \quad (15)$$

with $\gamma = 3/8$ (resp. $1/4$) for a uniform medium (resp. a stellar wind) and with t_p being the duration of the plateau. Then, combining equations (11–12–13–15) and the expression of e ,

$$e = \frac{1}{2} [1 - (1 - 2\gamma)^{1/2}]^2, \quad (16)$$

(Genet et al. 2007) we finally obtain

$$P_{\text{diss}}(t) = \frac{E_T}{t_p \varphi_{qq'}} F(\gamma) \left(\frac{t}{t_p} \right)^{\pm q\gamma - 1}, \quad (17)$$

with

$$F(\gamma) = \frac{\gamma}{2} [1 - (1 - 2\gamma)^{1/2}]^2. \quad (18)$$

The decay indices before and after the break at the end of the plateau are

$$\begin{cases} \alpha_1 = \gamma q - 1 \\ \alpha_2 = -\gamma q' - 1, \end{cases} \quad (19)$$

so that a flat plateau is expected for $q = 1/\gamma$ (i.e. $q = 8/3$ and 4 in the uniform medium and wind cases, respectively). For the examples shown in Fig. 3, equation (19) gives $\alpha_1 = -7/16$ and $-1/16$ for $q = 1.5$ and 2.5 (uniform medium) and $\alpha_1 = -1/4$ and $1/8$ for $q = 3$ and 4.5 (wind). If we impose a decay index $\alpha_2 = -1.5$ after the plateau we get the condition $q' = 1/2\gamma$ (i.e. $q' = 4/3$ and 2 for the uniform medium and wind cases, respectively). With our simple choice of $q = q'$ in Fig. 3 the decay is steeper when the plateau is flatter.

5 BUILDING A SEQUENCE OF MODELS

5.1 Forward shock scenario

It has been shown in Section 4.1 that a transition in the behaviour of ϵ_e (from rising to constant) at a fixed density n_0 marks the end of the plateau at a time t_p given by equation (5). The X-ray luminosity L_p at $t = t_p$ then writes from equations (3) and (4)

$$L_p \propto E^{\frac{p+2}{4}} t_p^{-\frac{3p-2}{4}} \propto t_p^{-p} \propto E_{\gamma, \text{iso}}^p \quad (20)$$

as long as the microphysics parameters at the end of the plateau and the gamma-ray efficiency do not vary much from burst to burst. Fig. 4(a) shows a sequence of afterglow light curves corresponding to different values of the isotropic gamma-ray energy release and the following choice of parameters: $\epsilon_e = 0.1 (n/n_0)^{-1}$ for $n > n_0 = 15 \text{ cm}^{-3}$ and $\epsilon_e = 0.1$ for $n < n_0$, $A_* = 0.5$, $p = 2.2$, $f_\gamma = 0.2$. It was obtained with a detailed calculation where the evolution of each elementary shocked shell is considered separately (Beloborodov 2005) except for the pressure, which is uniform throughout the whole shocked ejecta. The electron population and magnetic field of each newly shocked shell are computed taking into account the corresponding shock physical conditions and microphysics parameters. Then, each electron population is followed individually during the whole evolution, starting from the moment of injection, and taking into account radiative and adiabatic cooling. The resulting light curves somewhat differ from the simple analytical prediction of Section 4.1. The plateaus do not stay all flat, the brightest ones being slowly rising.

5.2 Reverse shock scenario

Using equation (10) it is possible to link the duration of the plateau to the gamma-ray energy release $E_{\gamma, \text{iso}}$ if Γ_* depends on the burst energy. A relation $\Gamma_H \propto E_{\gamma, \text{iso}}^{1/2}$ is suggested from the work of Liang et al. (2010) and Ghirlanda et al. (2012) based on the rising time

of the optical light curve, but Hascoët et al. (2014) have shown that it partially results from selection effects and has an intrinsic scatter much larger than originally inferred. Nevertheless we adopt $\Gamma_* \propto E_{\gamma, \text{iso}}^{1/2}$ for simplicity, keeping in mind a potential large dispersion, see Section 5.3. If moreover the gamma-ray efficiency

$$f_\gamma = \frac{E_{\gamma, \text{iso}}}{E_{\text{H}}} \quad (21)$$

does not vary much from burst to burst, we obtain

$$t_p \propto E_{\text{H}}^{-1} \propto E_{\gamma, \text{iso}}^{-1} \quad (22)$$

for both a uniform medium and a stellar wind. Together with equation (17) this fixes the dissipated power during the plateau phase

$$P_{\text{diss}} \propto t_p^{-2} \propto E_{\gamma, \text{iso}}^2. \quad (23)$$

To now compute a sequence of X-ray light curves from the dissipated power we have to fix the microphysics parameters ϵ_e and ϵ_B in the shocked material for which we adopt the fiducial values $\epsilon_e = 0.1$ and $\epsilon_B = 0.01$. The results for a uniform external medium of density $n = 1000 \text{ cm}^{-3}$ are shown in Fig. 4(b). We adopt this value as such large densities are expected in the immediate environment ($\lesssim 1 \text{ pc}$) of the massive progenitor star of a long GRB. They were obtained with the same method of calculation used in the forward shock case and outlined in Section 5.1. We start with a model having $E = E_{\text{H}} = E_{\text{T}} = 2 \cdot 10^{54} \text{ erg}$, $\Gamma_* = 16$, $q = 8/3$ and $q' = 4/3$ and then construct the sequence by multiplying or dividing E_{H} and E_{T} by the same factor F (i.e. we keep $E_{\text{H}} = E_{\text{T}}$) and simultaneously Γ_{H} and Γ_{T} by $F^{1/2}$. This prescription corresponds to $\Gamma_* = \Gamma_0 E_{\text{iso}, 53}^{1/2}$ with $\Gamma_0 = 35$. The sequence obtained for a stellar wind is similar, but due to the smaller contrast in Lorentz factor at the shock, the plateau flux is about three times smaller for the same value of the injected energy.

5.3 Prompt–afterglow correlations

When the sequences obtained in the previous section are transported back into the burst rest frame, the predicted correlations linking the plateau duration t_p , luminosity L_p , energy release in X-rays E_X and the isotropic gamma-ray energy $E_{\gamma, \text{iso}}$ can be compared to data. This is done in Fig. 5 for the $[L_p, E_{\gamma, \text{iso}}]$, $[t_p, E_{\gamma, \text{iso}}]$, $[L_p, t_p]$, $[L_p/E_{\gamma, \text{iso}}, t_p]$, $[E'_X, E_{\gamma, \text{iso}}]$ and $[E'_X/E_{\gamma, \text{iso}}, t_p]$ relations. Since the plateaus in observed bursts are not all flat contrary to our synthetic ones, we have replaced, for a simple comparison between data and models, the true X-ray energy release by the product $E'_X = L_p \times t_p$, both for model and data representative points. To account for the likely large dispersion of the $\Gamma_* \propto E_{\text{iso}, 53}^{1/2}$ relation (Hascoët et al. 2014), we also plot sequences corresponding to Γ_0 multiplied or divided by 3. Similarly, in the forward shock scenario we represent sequences where the wind parameter A_* has been multiplied or divided by 3. In some plots this dispersion has little effect, while in some others, especially $[t_p, E_{\gamma, \text{iso}}]$, it is quite large, but still compatible with the scatter of the data.

6 DISCUSSION AND CONCLUSION

We have addressed in this paper the origin of the plateau phase that is observed in about 50 per cent of the early afterglow light curves observed by *Swift* XRT (Nousek et al. 2006). We have shown that the commonly invoked cause of plateau formation by continuous energy injection into the forward shock leads to an efficiency crisis for the prompt mechanism as soon as the plateau duration exceeds 10^3 s .

We have then discussed two alternatives to energy injection, the first one still in the context of the forward shock scenario, the second in the more speculative one where the early afterglow is made by a long-lived reverse shock. Within the forward shock scenario a simple way to produce a plateau is to reduce the radiative efficiency of the shock by acting on the microphysics parameter ϵ_e . For a wind external medium a simple dependence of the form $\epsilon_e \propto n^{-1}$ for n larger than a critical density n_0 leads to the formation of a plateau approximately satisfying the prompt–afterglow correlations. The possibility of such a specific behaviour of ϵ_e remains to be confirmed but it is striking that the temporal evolution of only one parameter in the model can account for both the plateau formation and its phenomenology.

In the reverse shock scenario, the shape of the early afterglow is fixed by the distribution of injected power $\dot{E}_{\text{T}}(\Gamma)$ in the low Γ tail that is crossed by the shock. Using simple power laws for $\dot{E}_{\text{T}}(\Gamma)$ we have shown that flat plateaus and correct post-plateau decays can be obtained by adjusting the indices of the power laws. In addition, to satisfy the prompt–afterglow correlations the typical Lorentz factor of the ejecta should increase with burst energy. A relation of the form $\Gamma \propto E_{\gamma, \text{iso}}^{1/2}$, with a large scatter allowed, provides a reasonable fit of the data. Since the reverse shock is more efficient in a uniform rather than in a wind external medium, the same plateau luminosity can be achieved with three times less energy in the tail and we have then only presented results for this former case. The reverse shock scenario represents a true change of paradigm compared to the standard viewpoint. It has a much larger flexibility in terms of shapes of afterglow light curves. In addition to the capability to produce a plateau it can also account for various accidents such as bumps or steep slopes that are commonly observed (Uhm et al. 2012).

We have limited the present study to the X-ray light curves, and extending the analysis to the optical domain may help to discriminate between the forward and reverse shock scenario we have considered. However, a rich diversity of chromatic behaviours is observed between X-ray and optical domains (e.g. Melandri et al. 2008; Ghisellini et al. 2009; Panaitescu & Vestrand 2011; Li et al. 2012): (a) in a first class of events the optical light curve seems to track the X-ray light curve with similar pre-/post-break decay indices; see for example GRB 050801 (Rykoﬀ et al. 2006), GRB 060729 (Grupe et al. 2007) and GRB 090618 (Cano et al. 2011).² (b) Then in a second class of events, an optical break is observed in coincidence with the end of the X-ray plateau, but the pre-/post-break decay indices are somewhat different in X-ray and optical (e.g. Panaitescu 2007; Oates et al. 2011). (c) Finally, in a third class of events no clear optical break is seen in coincidence with the end of the X-ray plateau (e.g. GRB 050802; Oates et al. 2007).

Achromatic behaviours (class ‘a’) are most likely the result of a single source (i.e. the forward shock or the reverse shock), where electrons emitting optical and X-rays are in the same radiative regime. This is the case for the two sequences of synthetic GRBs shown in Fig. 4, where both X-rays and optical are produced in fast-cooling regime during the plateau phase.

As for chromatic behaviours, it is not clear whether they are the result of: (i) one single source where X-ray and optical emissions

² In some cases, achromatic breaks have been proposed to be the result of ‘jet breaks’ (e.g. Sari, Piran & Halpern 1999). This interpretation is however disfavoured for GRB 050801 and GRB 060729, as the measured post-break decay indices ($\alpha \simeq -1.5$) are typical and much shallower than predicted for a jet break.

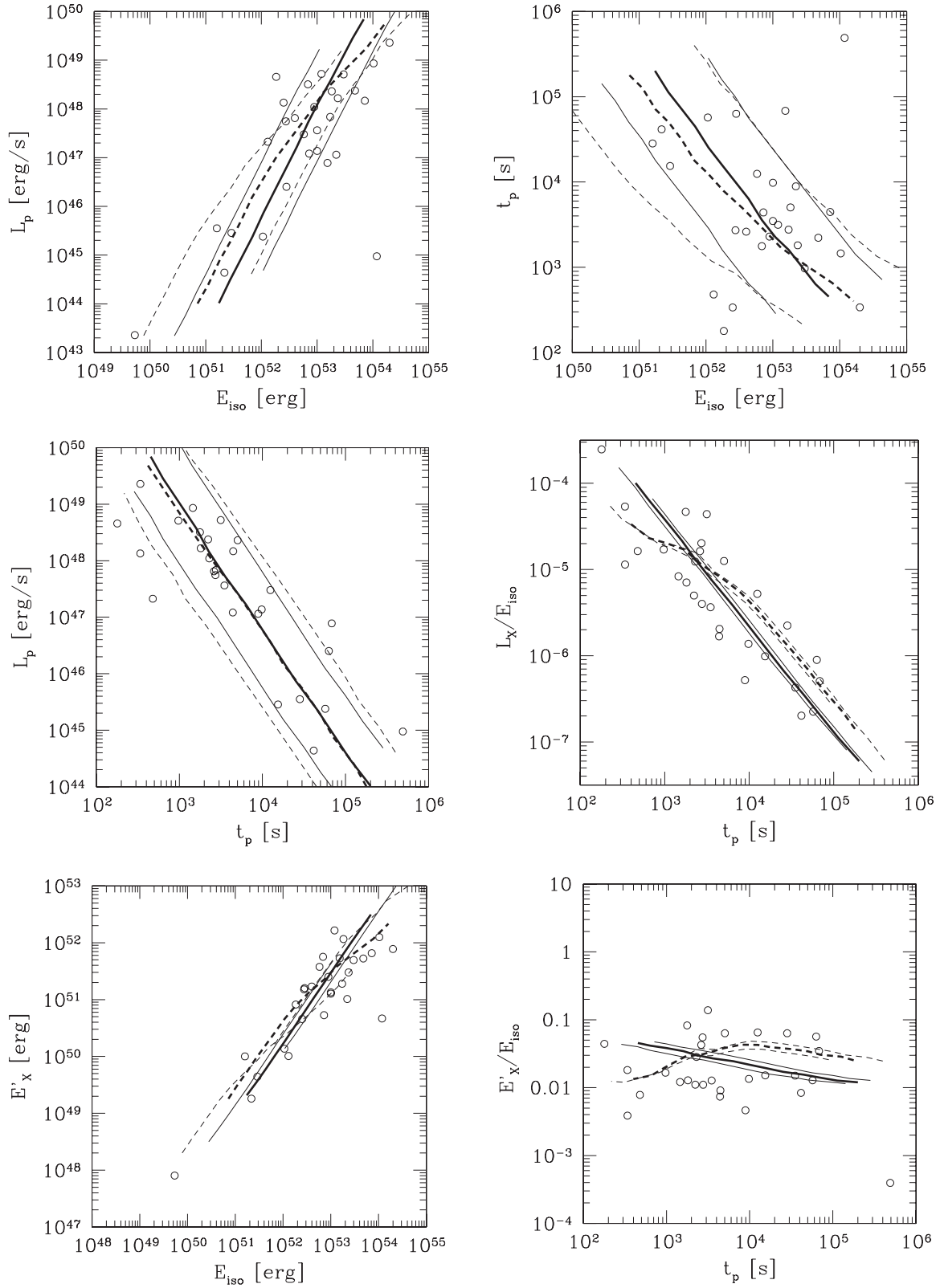


Figure 5. Prompt–afterglow correlations. Open circles show observations; error bars (not shown in this plot) are smaller than the intrinsic scatter of the samples. The thick full line corresponds to the forward shock case and the thick dashed line to the reverse shock case. The thin full and dashed lines, respectively, illustrate the effects of a factor of 3 dispersion in the wind parameter A_* and in the relation $\Gamma_* \propto E_{\gamma, \text{iso}}^{1/2}$ (see the text for details).

are produced in different radiative regimes. For instance, a situation where optical and X-ray emissions are, respectively, produced in slow-cooling and fast-cooling regimes (if the typical external density and/or ϵ_B are lower than assumed in the present study), can result in diverse chromatic behaviours. Slow-cooling regime will also make the optical emission much less responsive than X-rays to rapid variations in shock physics (microphysics or dynamics), as it is not dominated by freshly shocked electrons, which can smear out sharp transitions (e.g. breaks) that are well seen in X-rays. This has been investigated in the case of the reverse shock scenario by Uhm & Beloborodov (2007), Genet et al. (2007) and Uhm et al. (2012); (ii) two different sources, respectively, dominating in X-ray and optical domains. In the case where the X-ray plateau is produced by the forward (resp. reverse) shock, invoking the contribution of the reverse (resp. forward) shock will add freedom, which might be necessary in some cases (especially those belonging to class ‘c’). Due to this diverse phenomenology and the different possible interpretations, the extension to optical data would require a detailed modelling case by case, and we do not expect a unique signature of the models in the optical domain. The aim of the present study was first to obtain constraints on models imposed by the X-ray data and especially the prompt–early afterglow correlations.

ACKNOWLEDGEMENTS

It is a pleasure to thank Raffaella Margutti who kindly sent us her data on the prompt–afterglow correlations. This work has been financially supported by NSF grant AST-1008334 and the Programme National Hautes Energies (PNHE).

REFERENCES

Beloborodov A. M., 2005, *ApJ*, 627, 346
 Beloborodov A. M., 2010, *MNRAS*, 407, 1033
 Boër M., Gendre B., 2000, *A&A*, 361, L21
 Cano Z. et al., 2011, *MNRAS*, 413, 669
 Daigne F., Mochkovitch R., 1998, *MNRAS*, 296, 275
 Dainotti M. G., Ostrowski M., Willingale R., 2011, *MNRAS*, 418, 2202
 Dainotti M. G., Petrosian V., Singal J., Ostrowski M., 2013, *ApJ*, 774, 157
 Drenkhahn G., Spruit H. C., 2002, *A&A*, 391, 1141
 Gehrels N. et al., 2004, *ApJ*, 611, 1005
 Gendre B., Galli A., Boër M., 2008, *ApJ*, 683, 620
 Genet F., Daigne F., Mochkovitch R., 2007, *MNRAS*, 381, 732
 Ghirlanda G., Nava L., Ghisellini G., Celotti A., Burlon D., Covino S., Melandri A., 2012, *MNRAS*, 420, 483

Ghisellini G., Nardini M., Ghirlanda G., Celotti A., 2009, *MNRAS*, 393, 253
 Granot J., Königl A., Piran T., 2006, *MNRAS*, 370, 1946
 Grupe D. et al., 2007, *ApJ*, 662, 443
 Grupe D., Nousek J. A., Veres P., Zhang B.-B., Gehrels N., 2013, *ApJS*, 209, 20
 Hascoët R., Daigne F., Mochkovitch R., Vennin V., 2012, *MNRAS*, 421, 525
 Hascoët R., Beloborodov A. M., Daigne F., Mochkovitch R., 2014, *ApJ*, 782, 5
 Ioka K., Toma K., Yamazaki R., Nakamura T., 2006, *A&A*, 458, 7
 Kobayashi S., Piran T., Sari R., 1997, *ApJ*, 490, 92
 Liang E.-W., Yi S.-X., Zhang J., Lü, H.-J., Zhang B.-B., Zhang B., 2010, *ApJ*, 725, 2209
 Lithwick Y., Sari R., 2001, *ApJ*, 555, 540
 Li L. et al., 2012, *ApJ*, 758, 27
 Margutti R. et al., 2013, *MNRAS*, 428, 729
 Melandri A. et al., 2008, *ApJ*, 686, 1209
 Meszaros P., Rees M. J., 1997, *ApJ*, 476, 232
 Nousek J. A. et al., 2006, *ApJ*, 642, 389
 O’Brien P. T. et al., 2006, *ApJ*, 647, 1213
 Oates S. R. et al., 2007, *MNRAS*, 380, 270
 Oates S. R. et al., 2011, *MNRAS*, 412, 561
 Panaitescu A., 2007, *MNRAS*, 379, 331
 Panaitescu A., Kumar P., 2000, *ApJ*, 543, 66
 Panaitescu A., Vestrand W. T., 2011, *MNRAS*, 414, 3537
 Rees M. J., Meszaros P., 1994, *ApJ*, 430, L93
 Rees M. J., Meszaros P., 1998, *ApJ*, 496, L1
 Rees M. J., Mészáros P., 2005, *ApJ*, 628, 847
 Rowlinson A., O’Brien P. T., Metzger B. D., Tanvir N. R., Levan A. J., 2013, *MNRAS*, 430, 1061
 Rykoff E. S. et al., 2006, *ApJ*, 638, L5
 Sari R., Mészáros P., 2000, *ApJ*, 535, L33
 Sari R., Piran T., Narayan R., 1998, *ApJ*, 497, L17
 Sari R., Piran T., Halpern J. P., 1999, *ApJ*, 519, L17
 Shen R., Matzner C. D., 2012, *ApJ*, 744, 36
 Spruit H. C., Daigne F., Drenkhahn G., 2001, *A&A*, 369, 694
 Uhm Z. L., Beloborodov A. M., 2007, *ApJ*, 665, L93
 Uhm Z. L., Zhang B., Hascoët R., Daigne F., Mochkovitch R., Park I. H., 2012, *ApJ*, 761, 147
 Zhang B., Fan Y. Z., Dyks J., Kobayashi S., Mészáros P., Burrows D. N., Nousek J. A., Gehrels N., 2006, *ApJ*, 642, 354
 Zhang B. et al., 2007, *ApJ*, 655, 989

This paper has been typeset from a \LaTeX file prepared by the author.